Chapter 2

Previous Research and Scientific Background

Optical lithography has been the primary patterning technology for IC production for 30 years [1]. The death of optical lithography has been often predicted by industry pundits, incorrectly so far. At the present time, all non-optical lithography techniques are far behind the overall production capability of optical techniques [2]. Nonetheless, the fact remains that diffraction imposes limits on the potential of optical lithography. The critical dimension (CD) and depth of focus (DOF) limits of optical lithography can be given by the well-known Rayleigh equations [3, 4]:

$$CD = k_1 \frac{\lambda}{NA} \tag{2.1}$$

$$DOF = k_2 \frac{\lambda}{NA^2}, \tag{2.2}$$

where λ is the illumination wavelength, NA is the numerical aperture of the projection lens and k_1 and k_2 are system and process dependent parameters. There are two traditional ways to increase the spatial resolution of an optical system. The first approach is the shrinking of the illumination wavelength [5, 6, 7, 8, 9]. A large international research effort, informally coordinated by SEMATECH, is currently aimed at the transition from present 248 nm KrF excimer laser technology to the next generation 193 nm ArF excimer laser technology [10, 11, 12]. Pilot line tools will be available in 1999, and full production is likely to begin in the 2002 time frame. Applying high numerical aperture projection lens is the second approach to improve resolution. The practical limits of NA are probably in the 0.7 to 0.8 range, considering the difficulty of lens fabrication with the required low aberrations over large field sizes. However, the main limitation of these approaches is the decreased depth of focus. Many advanced and exotic techniques for enhancement of both the resolution and the depth of focus have been invented over the past 20 years (especially before a new generation is introduced), and a few of these have been developed quite extensively [13, 14]. The principal requirements for these techniques are: efficient resolution and DOF enhancement, low price, and minimal stepper modification. Figure 2.1 shows a schematic view of an optical stepper and the insertion points of some resolution enhancement techniques. A high intensity UV light source, such as a mercury arc lamp (g-line@436nm or i-line@365nm) or an excimer laser (KrF@248nm or ArF@193nm) is used to illuminate the photo-mask. The illumination beam is homogenized (producing a spatially uniform beam) and its spatial coherence is controlled by means of the filter of the condenser lens. Using special condenser filters, different **modified illumination** techniques (off-axis illumination *etc.*) can be introduced. The mask (or reticle) can be a simple binary chrome mask manufactured by e-beam technology. Optical proximity correction (OPC) masks are more complex chrome masks designed to compensate feature distortions (linewidth variation, line-end shortening *etc.*) that occur during imaging [15, 16, 17]. OPC masks improve the quality of the imaged pattern but do not enhance the resolution. **Phase shifting masks**, which apply different phase shifting layers on the mask, significantly improve the resolution.

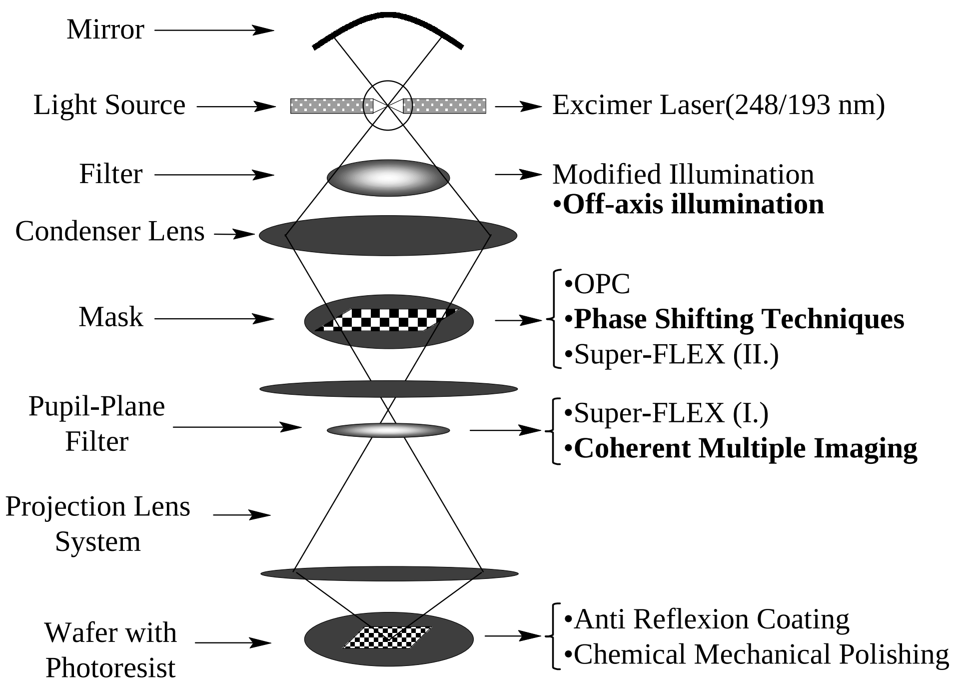

Figure 2.1: Schematic structure of an optical stepper and insertion point of some super resolution methods.

The most critical and expensive (> $1 million) part of a stepper is the projection lens. A modern stepper lens may be a meter in length and weigh 300 kg or more. The imaging performance of a lens is limited by diffraction ultimately, but aberrations could also degrade the lens performance. Pupil-plane filtering techiques (Super-FLEX *etc.*) introduce special amplitude-phase filters that modify the spatial Fourier components of the mask pattern. However, the feasibility of these methods is questionable, since the pupil-plane in microlithographic lenses is usually inaccessible. Application of top and bottom anti-reflexion coatings (ARC) could further improve the image quality minimizing the undesirable interference effects inside the photo-resist. The chemical mechanical polishing (CMP) method introduces an extra process step before every optical lithographic exposure. During this process the surface is polished, therefore the topology of the semiconductor structure does not limit the value of DOF seriously. A smaller limit in DOF means that projection lens with larger NA can be used, and larger NA means better resolution. The following four sections will focus on four super-resolution techniques that were the most important for my research.

2.1 Modified Illumination Techniques

2.1.1 Spatial Coherence

The control of spatial coherence which affects the resolution and the depth of focus, has historically been used to optimize the performance of a lithographic projection tool [18, 19]. Spatial coherence (σ) is defined as the ratio of the numerical apertures of the condenser and projection lens', respectively:

$$\sigma = \frac{NA_{condenser}}{NA_{projector}}. \tag{2.3}$$

Fully coherent illumination (σ=0) means that the mask is illuminated by a normally incident plane wave. In this case the adjacent patterns interfere and undesirable high intensity peaks could appear. The illumination is incoherent if the incident angle of the continuous spectrum of plane waves ranges from -90° to +90°. If the incident plane waves have a finite range (smaller than 90°) then the illumination is called partially coherent. A typical value of spatial coherence in optical microlithography is around σ=0.5. The value of spatial coherence can be easily controlled by means of an adjustable aperture in the condenser. Using partially coherent illumination the modified Rayleight resolution limit is [20]:

$$CD = k_1 \frac{\lambda}{NA(1+\sigma)}, \tag{2.4}$$

and the depth of focus for line-space patterns can be given as :

$$DOF = k_2 \frac{\lambda}{\left(1 - \sigma + \frac{\sigma^2}{2}\right) NA^2} \qquad if \quad pitch = \frac{\lambda}{NA}, \tag{2.5}$$

$$DOF = k_2 \frac{\lambda}{\left(1 + \left(\frac{\lambda}{pitch \cdot NA} - \sigma\right)^2\right) NA^2} \qquad if \quad \frac{1}{2}\frac{\lambda}{NA} < pitch < \frac{\lambda}{NA}, \tag{2.6}$$

where the pitch size means the period of a line/space pattern (line width + line separation). Optimization of spatial coherence is an important task in advanced lithography. However, it is very difficult to arrive at an absolute statement, since it strongly depends on the type of the structure. While the optimal imaging of contact holes requires relatively small σ, using equal line/space structures better imaging performance can be obtained with higher σ value. In the present time every major manufacturer of step-and-repeat projection lithography tools has introduced a "flexible" stepper, a model with variable numerical aperture and spatial coherence.

2.1.2 Off-axis Illumination

The three-dimensional aerial image of a lithographic projection system is influenced by the method of illumination [21, 22, 23]. In classical projection systems, Köhler configuration [24] is generally applied to illuminate the photo-mask. In this method the source is imaged into the entrance pupil of the projection lens. Fig. 2.2 depicts a comparison of conventional and off-axis illumination for line/space patterns. Using a conventional illumination system, line/space patterns can be resolved if at least three (the zero and the ± 1) diffraction orders contribute to the final aerial image. Using a lens close to its resolution limit, the ± 1 diffraction orders transmit through the edge of the aperture, while the higher intensity zero order falls in the middle of the aperture. The intensity ratio of the beam diffracted into the zero and first orders for an ideal equal line/space pattern (Ronchi grating) is known to be $1 : (2/\pi)^2$, resulting in an image contrast of:

$$C = \frac{I_{max} - I_{min}}{I_{max} + I_{min}} = \frac{\left(1 + \frac{2}{\pi}\right)^2 - \left(1 - \frac{2}{\pi}\right)^2}{\left(1 + \frac{2}{\pi}\right)^2 + \left(1 - \frac{2}{\pi}\right)^2} = 90.6\%. \tag{2.7}$$

And the cut-off frequency of the system is:

$$f_{cut-off} = \frac{1}{2}\frac{\lambda}{NA}. \tag{2.8}$$

The second and higher diffraction orders are not transmitted by the lens, and they do not contribute to the final image. Obviously, for features with a pitch size larger than λ/NA, higher diffraction orders must be considered.

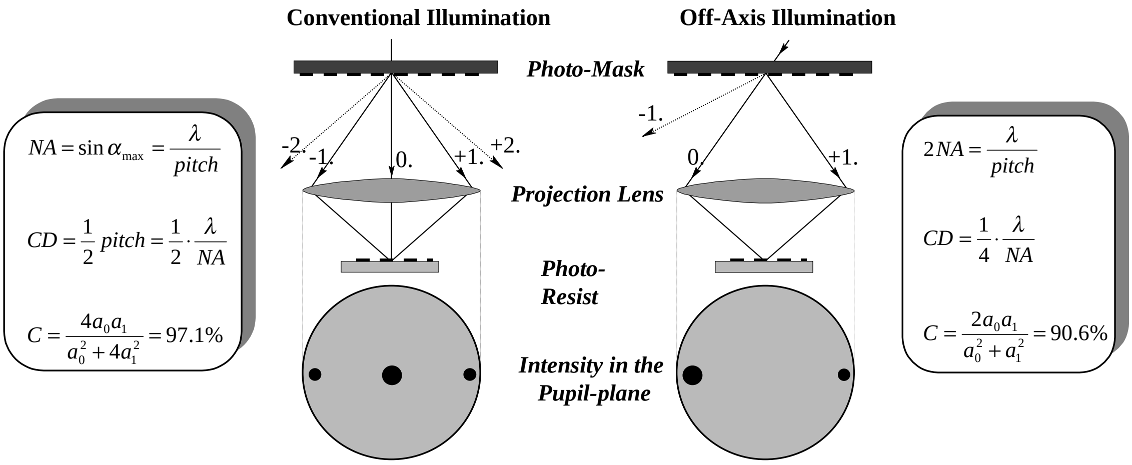

Figure 2.2: Comparison of conventional and off-axis illumination.

For off-axis illumination, the zero-order Fourier component of a mask pattern produces an off-axis spot of light in the pupil of the projection lens. One of the first-order diffraction spots appears nearly symmetrically on the other side of the optical axis, and the other first-order diffraction spot is lost. In an optimum case the cut-off frequency improved to

$$f_{cut-off} = \frac{1}{4}\frac{\lambda}{NA}, \tag{2.9}$$

so that the smallest resolvable feature size doubled. However, the contrast of the image degraded to 0.90, owing to the intensity difference between the zero and the first diffraction orders. Off-axis illumination improves both the resolution and depth of focus of periodic patterns, however the effect of the illumination on the performance of isolated lines is very small. "Two beam imaging" degrades the image contrast and reduces the illumination power.

For most integrated circuit applications, features are limited to horizontal and vertical orientation, and a quadrupole configuration may be more suitable. Poles are now only at diagonal positions with respect to horizontal and vertical mask features, and each pole is off-axis to all mask features.

2.2 Phase Shifting Techniques

Control of the phase information at a mask may allow for the manipulation of the imaging performance. Phase shift masking uses destructive and/or constructive interference to improve the image quality of different feature types [25, 26].

2.2.1 Phase Shifting Techniques Using Phase Shifting Masks

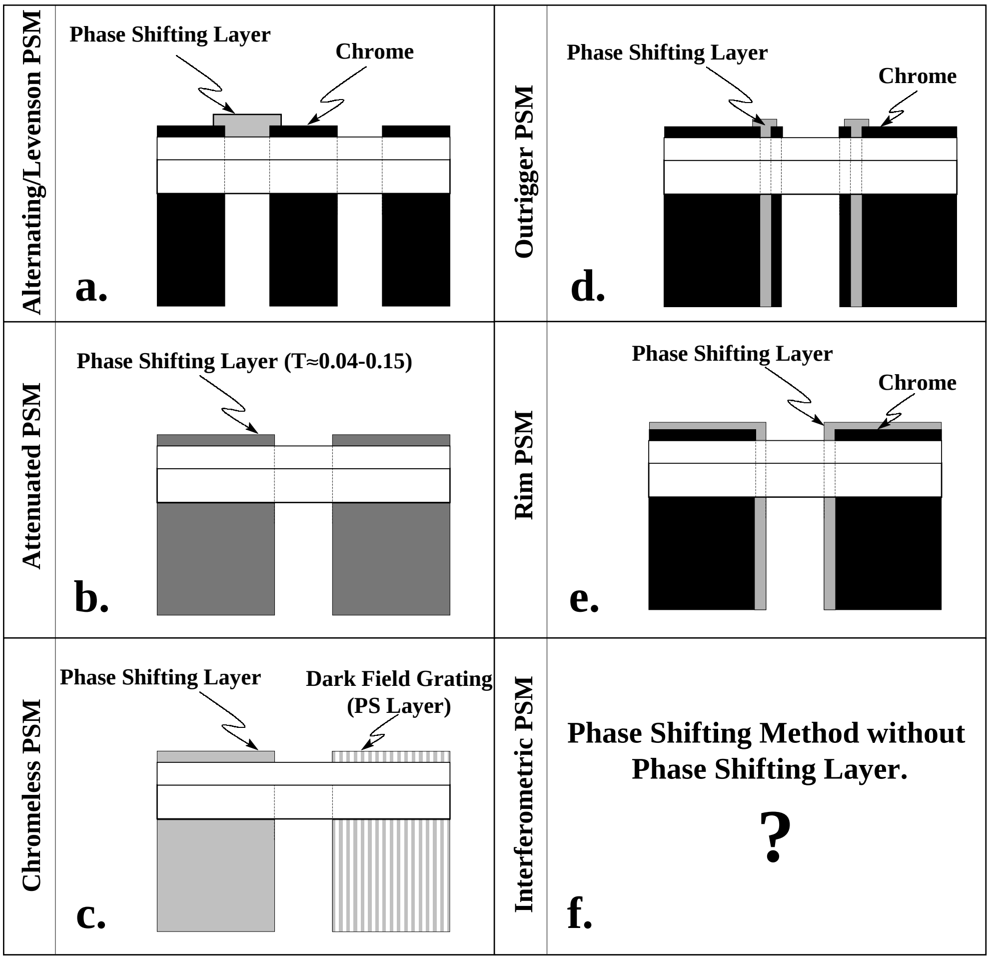

Figure 2.3: Phase shifting techniques.

Fig. 2.3 depicts five different phase shifting methods. The alternating phase shifting mask (Fig. 2.3.a) proposed by Levenson and Shibuya in 1982 [27, 28], introduces a π phase difference between adjacent features. Due to destructive interference between opposite fields, the final aerial image performance could be improved. In case of equal line-space patterns, the zero order disappears and just the higher diffraction orders contribute to the aerial image. In an optimum case, when the feature size is close to the resolution limit of the optical system, only two diffraction orders (the ±1 ones) generate the image. However, this kind of "two beam" imaging does not degrade the image contrast, since the intensity of the ±1 diffraction orders is equal. The alternating phase shifting method is a very candidate technique to improve the resolution and the depth of focus of periodic structures. However, designing alternating phase shifting masks to produce nonperiodic circuit patterns has proven difficult. To overcome this problem new phase shifting approaches were developed that are able to improve the image quality of both line-space patterns and isolated lines. The attenuated phase shifting method (see Fig. 2.3.b) is by far the most candidate technique [29]. The mask structure is simple; it contains only clear and attenuated/phase-shifting areas, respectively. The typical value of attenuation is in the range of 4 to 15%. Chromeless phase shifting masks (Fig. 2.3.c) contain only clear and phase shifted areas. Despite the fact that the phase shifting layer is transparent at the applied wavelength, dark areas, called dark field gratings can be produced. The period of these gratings is smaller than the resolution limit of the projection lens. The first diffraction orders fall outside the aperture, and no light diffracted on the dark field grating could pass through the lens. The outrigger and rim phase shifting techniques (Fig. 2.3.d-e) are two other alternative solutions for image quality improvement. Besides their advantages, the phase shifting methods suffer from several issues that limit their applicability in optical microlithography [30, 31, 32, 33]:

1. Phase shifting mask design and optimization is a complex process.

2. Phase shifting mask manufacturing is a complicate, multi-step process. The deviation from the optimum phase value cannot be larger than 5°.

3. Phase shifting mask repair is an important process since the printability of transparent phase shifting defects is significantly higher than the printability of opaque defects. Cleaning technologies are expensive and require special equipment.

Problems introduced by the phase shifting layers could be overcome by means of a new phase shifting technique that does not apply any phase shifting layers on the mask.

2.2.2 Phase Shifting Method Without Phase Shifting Mask - Interferometric Phase Shifting Technique

The interferometric phase shifting technique ($IPST$) proposed by Szabo, and demonstrated by Kido in 1994 [34], uses a simple chrome mask that is illuminated from the front and the back sides using a Mach-Zehnder interferometer (see Fig. 2.4).

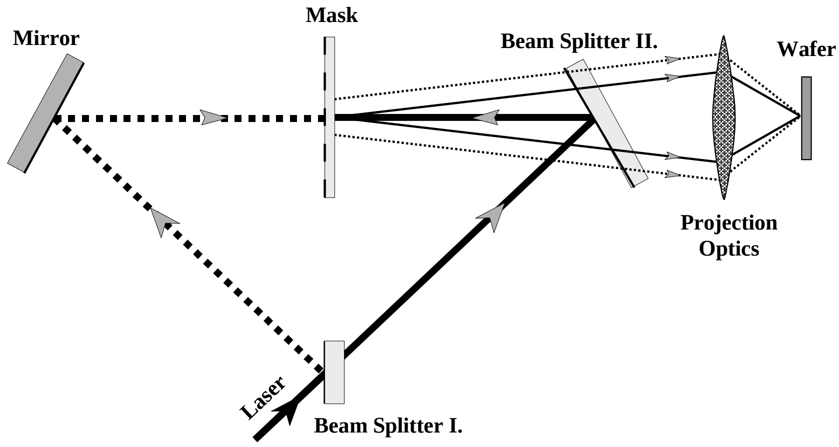

Figure 2.4: Interferometric phase shifting technique.

The value of the phase shift between reflected and transmitted beams could be controlled by the translation of the interferometer mirrors. The amplitude ratio can also be aligned using a continuous attenuator in one arm of the interferometer. Theoretical and experimental results proved that the interferometric phase shifting technique has the similar resolution and depth of focus enhancement potential as the attenuated phase shifting technique. Since $IPST$ requires optics with high surface quality, the thickness of the beam-splitter placed between the mask and projection lens is in the range of several centimeters. Such a thick and tilted plane-parallel plate introduces serious optical aberrations (astigmatism, spherical aberration and coma) into the system [35].

2.3 Filtering Methods

Changing the amplitude and/or the phase condition of the transmitted light in the aperture of the projection lens is a traditional method to enhance the aerial image quality.

2.3.1 Image Formation Based on Fourier Optics

Aerial image calculation in photolithographic simulation tools such as in Prolith/2 or in Solid-C is based on Fourier optics [36, 37], wherein the resultant electric field profile is calculated as an inverse Fourier transform of the product of the Fourier transform of the mask pattern ($m(x, y)$) and the coherent transfer function of the optical system

$(P(f_x, f_y))$:

$$E(x,y) = \mathfrak{F}^{-1}\{\mathfrak{F}\{m(x,y)\} \cdot P(f_x, f_y)\}, \tag{2.10}$$

where (x, y) are spatial coordinates, (f_x, f_y) are spatial frequencies, and $\mathfrak{F}$ and $\mathfrak{F}^{-1}$ represent the Fourier and inverse-Fourier transforms, respectively. The properties of the optical projection system (numerical aperture, optical aberrations, pupil-plane filter *etc.*) can be described by means of the coherent transfer function. Advanced simulation software is able to controll the spatial coherence of the illumination.

2.3.2 Pupil-Plane Filtering Techniques

The final image quality can be modified by introducing a filter into the Fourier plane of the projection system (pupil plane filter). A complex filter changes the phase and amplitude condition between the spatial Fourier components of the mask pattern, and therefore has a deep influence on the aerial image.

The first major application of pupil-plane filtering technique in optical microlithography is linked with the name of Fukuda. In 1991 [38, 39] he proposed a method called Super-FLEX that could effectively enhance the depth of focus by a factor of 3, and yields a resolution enhancement of 20% using contact hole patterns. The principle of the Super-FLEX method is described in the following.

Assuming coherent illumination, the electric field $(E_0(x, z))$ of an image in the lateral x, and axial z directions can be described by the equation of

$$E_0(x,z) = e^{i\phi(z)} \cdot \int M(f) \cdot P_0(r,z) \cdot e^{2\pi i f x} df, \tag{2.11}$$

where $\phi(z)$ is the phase of the light $(= 4\pi z/NA^2)$, f is the spatial frequency normalized by NA/λ, $M(f)$ is the spatial Fourier transform of the mask pattern, $P_0(r, z)$ is the coherent transfer function of the system and the defocus (z) is normalized by $2\lambda/NA^2$. The coherent transfer function can be written as

$$P_0(r,z) = circ(r) \cdot e^{2\pi i z r^2}, \tag{2.12}$$

where r is the radial coordinate on the pupil-plane normalized by the pupil radius. The superimposed electric field (E_{total}) of two images defocused by $z = \pm\beta$ and phase shifted by $\pm\Delta\phi$ can be written as

$$E_{total}(x,z) = \frac{1}{2} \cdot \left[e^{i\Delta\phi} \cdot E_0(x, z-\beta) + e^{-i\Delta\phi} \cdot E_0(x, z+\beta) \right]. \tag{2.13}$$

Substituting Equation (2.11) into Equation (2.13) the total electric field can be expressed as

$$E_{total} = e^{i\phi(z)} \cdot \int M(f) \cdot P_0(r,z) \cdot cos(2\pi\beta r^2 - \frac{\theta}{2}) \cdot e^{2\pi i f x} df, \tag{2.14}$$

where

$$\theta = 2\Delta\phi - \frac{8\pi}{NA^2}\beta. \tag{2.15}$$

The $cos(2\pi\beta r^2 - \frac{\theta}{2})$ term can be explained in two different ways. First, the "extra" term belongs to the coherent transfer function and it can be considered as a pupil-plane filter (Super-FLEX I or spatial filtering method). Second, the "extra" term is connected to the mask function (Super-FLEX II or mask modulation method). The new mask is obtained by the inverse-Fourier transform of $M(f) \cdot cos(2\pi\beta r^2 - \frac{\theta}{2})$. This second approach can be considered as a special optical proximity correction (OPC) technique.

However, in practice it is rather difficult to produce a pupil-plane filter or photo-mask with a complex and continuous transmission/phase distribution. Therefore simplified filters and masks were used for the evaluation of the performance of Super-FLEX. It was shown that both approaches enhance the image quality in the same manner. The main limitation of the Super-FLEX method is that a pupil-plane filter cannot be inserted into a modern lithography stepper without significant system modification that reduces the lens performance.

In 1992 von Bünau et. al. [40] optimized an amplitude transmission pupil-plane filter that produced an approximately constant on-axis intensity profile, while maintaining a large value of energy within the central peak. The calculation applied scalar wave and paraxial approximations regarded to the point-spread function of the optical system. More complex patterns were not evaluated. The optimized amplitude filters were so complex that their technical feasibility was questionable.

In 1995 Horiuchi et. al. [41] also used a transmittance-adjusted pupil-plane filter to image different line-space patterns simultaneously. They managed to address some imaging issues (pattern-end degradation and shrinkage in middle size patterns) by optimizing the radii of the transmission zones of the pupil-plane filter.

2.3.3 Annular Illumination

The intensity distribution near the focus of a projection lens with circular and annular apertures has been theoretically investigated by several authors [42, 43, 44]. This section summarizes the most important theoretical results.

Consider a lens of focus length f and let it be illuminated by plane waves of wavelength λ. The radius of the lens aperture is R. To describe the intensity distribution near the focus two variables u and v are introduced which are defined as:

$$u = \frac{2\pi R^2}{\lambda f^2} z, \qquad v = \frac{2\pi R}{\lambda f} r, \tag{2.16}$$

where r is the polar coordinate ($r^2 = x^2 + y^2$), and z is the axial distance from the focus point.

The intensity distribution in the geometrical focal plane (u=0) is given by the well-known Airy pattern:

$$I(0, v) = \frac{4\pi^2 R^4}{\lambda^2 f^2} \left(\frac{2J_1(v)}{v} \right)^2, \tag{2.17}$$

where J_1 is the first order Bessel function. The v value characteristic of the first dark ring is 3.832. Thus the resolution power can be given as:

$$CD = 0.61 \cdot \frac{\lambda}{NA}, \quad where \quad NA = \frac{R}{f} \quad \boxed{\Rightarrow \mathbf{k_1 = 0.61}}. \tag{2.18}$$

The intensity distribution along the optical axis ($v = 0$) is:

$$I(u, 0) = \frac{4\pi^2 R^4}{\lambda^2 f^2} \left(\frac{sin(\frac{1}{4}u)}{\frac{1}{4}u} \right)^2. \tag{2.19}$$

The argument of the sine function equals π in the case of the first minimum. DOF can be expressed as the distance between the first minimum and the main maximum:

$$DOF = 2 \cdot \frac{\lambda}{NA^2} \quad \boxed{\Rightarrow \mathbf{k_2 = 2}}. \tag{2.20}$$

If the central portion of the exit pupil is blocked out so that the aperture consists of an annulus between circles R and ϵR – the obstruction ratio (ϵ) can vary in the range from 0 to 1 – the intensity distribution in the focal plane becomes:

$$I(0,v) = \frac{4\pi^2 R^4}{\lambda^2 f^2} \cdot \left(\frac{2J_1(v)}{v} - \epsilon^2 \frac{2J_1(\epsilon v)}{\epsilon v} \right)^2 . \tag{2.21}$$

Equation (2.21) shows that the diffraction pattern of an annular ring is the diffraction pattern of the whole aperture extending to the outer circumference, minus that of the inner, opaque region. An increase of ϵ leads to a decrease in the radius of the first dark ring. As ϵ tends to unity, the expression inside the bracket of Equation (2.21) tends to $(1-\epsilon^2)J_0(v)$, where $J_0(v)$ is the zero order Bessel function of the first kind. In the limiting case the $FWHM$ of the Bessel beam is 1.6 times smaller than the $FWHM$ of the Airy pattern. The intensity distribution along the optical axis can be given as:

$$I(u,0) = \frac{4\pi^2 R^4}{\lambda^2 f^2} \cdot \left(\frac{sin\frac{1}{4}u(1-\epsilon^2)}{\frac{1}{4}u} \right)^2 . \tag{2.22}$$

A comparison of Eq. (2.22) with Eq. (2.18) indicates that the separation of the successive dark points on the optical axis is increased by a factor of $1/(1-\epsilon^2)$, and tends to infinity as ϵ tends to unity. Equations (2.21) and (2.22) show that the DOF and resolution can be enhanced simultaneously using an annular aperture. One of the main issues of this technique is that an n-fold gain in focal depth leads to an n-fold loss in the intensity of the illumination light.

2.3.4 Coated Objective

The theoretical investigation of the resolving power of a coated objective dates back to nearly 50 years [45, 46, 47]. The problem of coating the objective in order to obtain a diffraction pattern having the smallest central bright spot was studied by John W. Y. Lit in 1971 [48]. He pointed out that the diffraction pattern in the focal plane of the lens has the smallest bright spot when the aperture is divided into two zones, with the inner zone having a phase retardation of π rad with respect to the outer one. The transmission of both parts is unity. The total complex disturbance $E(P)$ near the focus using a simplified two-zone annulus shown in Fig. 2.5 is:

$$E(P) = \frac{ikR^2}{f} e^{ik(f-OP)} \{ T \int_0^1 e^{\frac{1}{2}iu\varrho^2} J_0(v\varrho)\varrho d\varrho + (T'-T)\epsilon^2 \int_0^1 e^{\frac{1}{2}iu'\varrho^2} J_0(v'\varrho)\varrho d\varrho \} \tag{2.23}$$

where: $u = kR^2 z/f^2$, $v = krR/f$, $k = 2\pi/\lambda$, $r = (x^2+y^2)^{1/2}$, ϱ is the radius vector in the observation surface, O is the geometrical focus, and T and T' are the amplitude

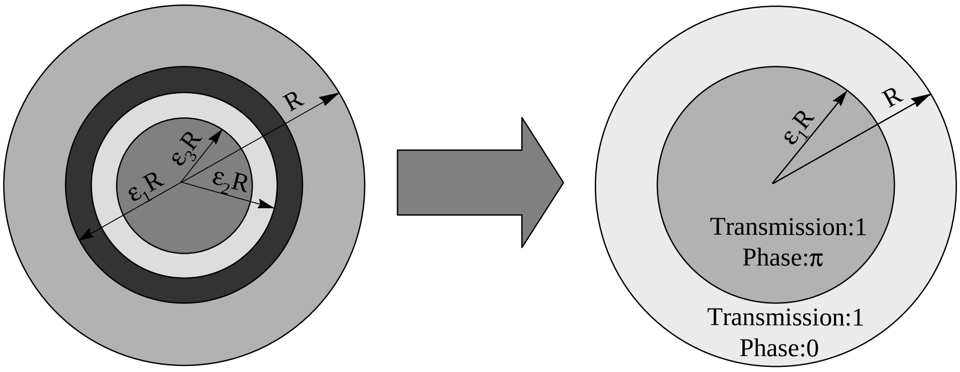

Figure 2.5: General and simplified two-zone annulus

transmittance of the outer and the inner zones, respectively. With respect to $T = e^{i0} = 1$ and $T' = e^{i\pi} = -1$, the intensity in the geometrical focal plane ($u = 0$) and along the optical axis ($v = 0$) can be given as

$$I(0,r) = \frac{\pi^2 R^4}{\lambda^2 f^2}\left[\frac{2J_1(v)}{v} - 2\epsilon^2 \frac{2J_1(\epsilon v)}{\epsilon v}\right]^2, \tag{2.24}$$

$$I(z,0) = \frac{\pi^2 R^4}{f^2 \lambda^2}\left[2(1-\epsilon^2)^2\left(\frac{sin1/4u(1-\epsilon^2)}{1/4u(1-\epsilon^2)}\right)^2 - \left(\frac{sin1/4u}{1/4u}\right)^2 + 2\epsilon^4\left(\frac{sin1/4\epsilon^2 u}{1/4\epsilon^2 u}\right)^2\right]. \tag{2.25}$$

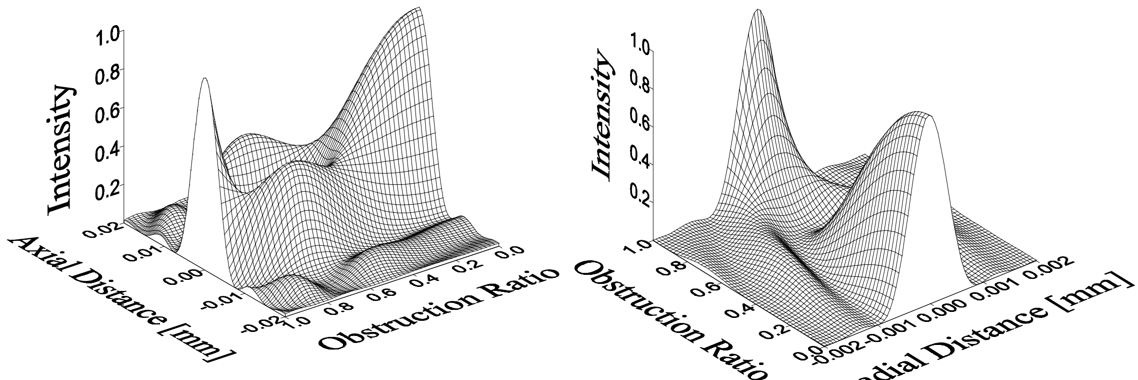

Figure 2.6: Intensity distribution in the focal plane and along the optical axis related to the obstruction ratio. ($R = 5mm; f = 25mm; \lambda = 632nm$)

The obstruction ratio strongly determines the intensity distribution in the focal region. In the case of ϵ=0 and ϵ=1 the intensity distribution on the focal plane is the well-known Airy pattern. If the obstruction ratio is increaded, the intensity of the main central peak begins to decrease and reaches its minimum value (=0) when ϵ=0.7. In this case the area of the central circle equals to the area of the surrounding ring ($\epsilon = 1/\sqrt{2}$). If the value of ϵ is further increased, the intensity of the central peak begins to increase again. The intensity of the first diffraction ring grows continuously if ϵ increases. The intensity distribution on the optical axis related to ϵ is also depicted. In case of ϵ=0 and ϵ=1 the axial intensity distribution can be described by a $(sin(x)/x)^2$ function. There is a range of ϵ where two foci appear. If we use the definition that DOF is the axial distance between the central main peak and the first minimum, a coated objective always has a larger DOF than an uncoated one, except when ϵ=0.7.

2.4 Nondiffracting Beams

Non-diffracting beams represent a group of fields whose radial intensity distributions do not change during their propagation. In 1987 Durnin [49] showed that the field described by

$$E(r, z, t) = A \cdot J_0(k_\perp r) \cdot e^{i(k_\parallel z - \omega t)} \tag{2.26}$$

is an exact solution of the wave equation, where $k_\perp^2 + k_\parallel^2 = \omega^2/c^2$, and J_0 is the zero order Bessel function of the first kind. The field described by Eq. (2.26) represents a non-diffracting beam because the transverse intensity distribution is independent of the propagation distance (z). However, such an ideal beam cannot be realized experimentally over large values of z and r, since this would represent a beam with infinite energy and spatial extent [50].

In the last twelve years several experimental arrangements have been proposed to create nearly non-diffracting Bessel beams and apply them in different domains of physics [51, 52, 53, 54, 55]. The first arrangement to create a nearly nondiffracting Bessel beam was also suggested by Durnin [56]. A circular slit (annular aperture) was placed at the focal plane of a lens. The slit was illuminated with collimated light. Each point-like source along the slit was transformed by the lens into a plane wave whose wave vector lies on the surface of a cone around the optical axis. The maximum z value, for which the plane waves intersect and thus form a nondiffracting beam, was $Z_{max} = D/tan\Theta$, where D is the radius of the circular aperture, and Θ is the angle that k vector makes with the z axis ($tan\Theta = k_\perp/k_{parallel}$). The maximum range of the J_0 beam that could be realized experimentally was 85 cm, and it could be fitted by numerical simulations. In 1992 Cox et. al., [57, 58] based on the theoretical considerations by Indebetouw

[51], produced a similar nondiffracting beam using a Fabry-Perot interferometer. The ring system transmitted by the Fabry-Perot interferometer was collimated by a lens. An annular aperture placed at the focal plane of the lens transmitted only the first ring and blocked all the others. A second lens located after the spatial filter had the same role as in the experiment reported in Ref [56]. It can be seen that the effective nondiffracting range using such a setup is $Z_{max} = 2Fd$, where F and d are the finesse and the thickness of the etalon, respectively. In fact, nondiffracting beams have also been generated by means of an axicon [59, 60], a holographic process [61, 62], and a new type of laser cavity. It is worth noting that already a century ago it was recognized that the diffraction pattern of a very narrow annular aperture can be described by the J_0 function. However, previous work paid less attention to the depth of focus and therefore did not describe such patterns in terms of nondiffracting beams. Only a few applications of nondiffracting beams have been reported so far.